Supplement of Atmos. Chem. Phys., 25, 10661–10675, 2025
https://doi.org/10.5194/acp-25-10661-2025-supplement

Supplement of

Sectoral contributions of high-emitting methane point sources from major US onshore oil and gas producing basins using airborne measurements from MethaneAIR

Jack D. Warren et al.

Correspondence to: Jack D. Warren (jwarren@edf.org) and Ritesh Gautam (rgautam@edf.org)

S1. Thresholding method used to identify methane plumes in MethaneAIR scenes.

The gridded flux map used to identify methane plumes is shown in Figure S1.1. The left panel shows the 600m x 600m boxes being tiled across the XCH4 image, and the DI is calculated around each box using HRRR winds to estimate the flux from within the box. The DI method has been described in Chulakadabba et al., 2023; briefly, it is based on Gauss's divergence theorem applied to surfaces enclosing a source. The surface integral is estimated based on XCH4 measurements along a square or rectangle:

$$\Phi_{\text{surf}} = \sum^{\text{around rect}} \left(\text{XCH4}_i - \langle \text{XCH4} \rangle_{\text{rect.}}\right) \cdot n_{\text{column}} \cdot M_{\text{CH}_4} \cdot v_{\text{perpendicular}} \cdot \Delta l + \left\langle \frac{\partial m}{\partial t} \right\rangle,$$

where Φ_{surf} is the flux (kg/h) into the enclosed volume from the land surface, XCH4_i is an individual measurement along the rectangle, $<\text{XCH4}>_{\text{rect}}$ is the mean of all measurements along the rectangle, Δl is the distance between successive XCH4 measurements, n_{column} is the moles of air in the column based on the surface pressure from HRRR, M_{CH4} is the molar mass of methane, $v_{\text{perpendicular}}$ is the wind speed perpendicular to the sides of the rectangle, and $<\partial m/\partial t>$ is the rate of change of total mass in the enclosed volume (~0 for plume-size volumes). A box size of 600m was chosen as it is a typical plume width that we observed, so the boxes are on the scale of a plume, and can fully enclose a plume's origin. The boxes are oversampled (not shown in the figure), moving the box over by 200m in each step, to produce a gridded flux product on a 200m x 200m grid (Figure S1.1, right panel).

Note that while the methane plume in the left panel extends across the length of the figure, in the right panel the upwind end near the source produces much higher (and lower) flux values than the downwind end, which helps us identify the plume source. While the gridded flux product was quite useful on the plume scale, we found that summing totals across the scene was not accurate at estimating regional emissions, as some assumptions in the method, such as no significant mass loss through the top and bottom of the box, were not valid in the large scale, but were valid on the scale of individual plumes. We use HRRR winds at level 3, ~80m, which is the typical mixing height of a plume on length scales of 100-2000 m from the source, which is the scale at which we typically observe plumes with MAIR.

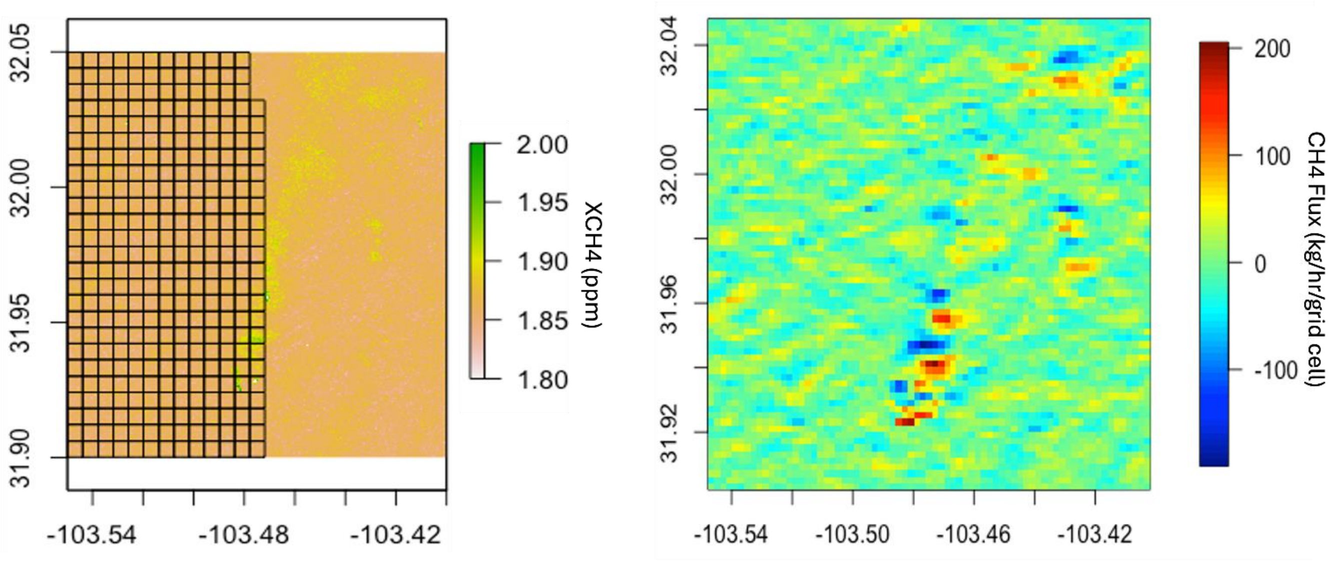

Figure S1.1 Left: 600 m grid used to calculate divergence integral (DI) for a small area of flight RF06. DI is calculated to find the flux through each box. Oversampling is used by moving sequentially moving the 600m box over by 200m across the scene, producing the 200m gridded image to the right. Right: Gridded DI flux product corresponding to MethaneAIR scene on the right.

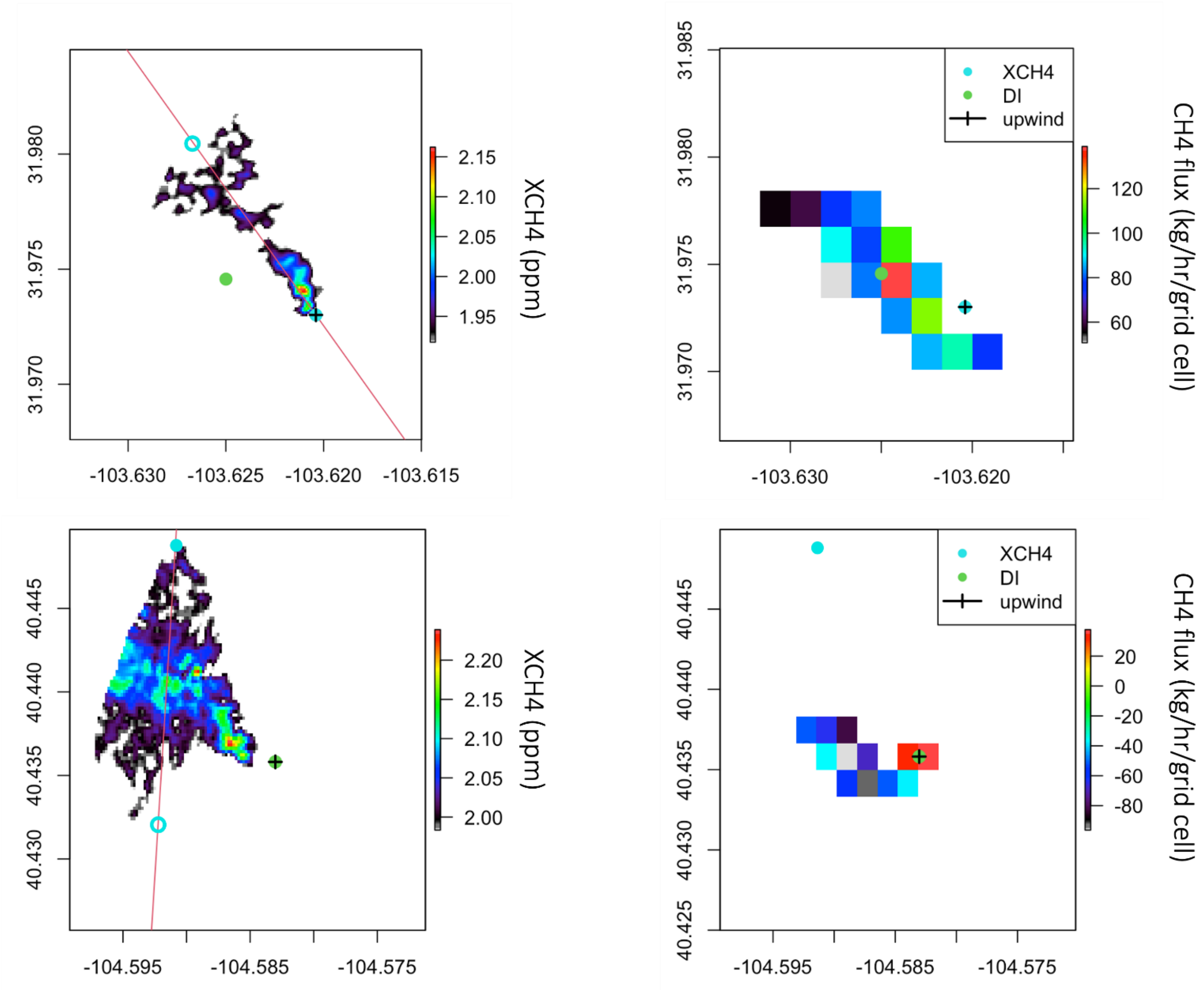

Figure S1.2 Left column: Masked XCH4 plumes. Right column: Masked DI flux "clumps". Red line shows the major axis of the XCH4 plume. The top and bottom rows show 2 different plumes. The filled and open cyan circles are the upwind and downwind ends of the plume, respectively, based on the ends of the XCH4 mask along the major axis, and the HRRR wind direction. The green circle is the center of mass of the positive portion of the DI flux "clump". The plus is the point chosen as the origin of the plume, whichever is upwind between the upwind end of the XCH4 mask and the center of the DI flux clump.

Figure S1.2 shows 2 sample masked plumes found with our plume-finding method. To locate plumes in the scene, we first took the absolute value of the gridded flux map, as inaccuracies in the meteorological product's wind direction often lead to positive and negative dipoles around plumes. We identified and isolated "clumps" of elevated [absolute value of] flux by defining a threshold of 1.3*[standard deviation of scene's gridded flux] + [mean of scene's gridded flux], and setting values below that threshold to null values; to keep a clump it must have at least 12 200 m x 200 m pixels. The isolated flux "clumps" are shown on the right of Figure S1.2. The mask is based on the absolute value of the flux, but the true fluxes (positive and negative values) are shown here. The center of mass of the positive pixels of the DI clump is shown as a green dot. A flux "clump" is only considered to be a plume if it also has an XCH4 "clump" within ± 3 km, with >200 connected 10 m × 10 m pixels that are above 1.3*[standard deviation of cropped scene's XCH4] + [mean of cropped scene's XCH4].

The XCH4 plume masks associated with the elevated DI clumps are shown on the left of Figure S1.2. We find the long axis of the plume mask, which is shown as a red line. Using the HRRR wind direction, we find the upwind and downwind ends of the plume mask along its long axis, which are marked with filled and open cyan circles, respectively. The top row is a typical plume form, where the upwind end of the plume is correctly found to be the plume origin. The bottom row shows a wide plume, which is near the edge of the scene, cropping its downwind extent. Our algorithm therefore finds the long axis of the plume which is actually perpendicular to the wind direction. The long axis of the plume mask may also be perpendicular to the wind direction under low wind speeds, when "pancake"-shaped plumes can form. Because of such cases, where the cyan dot does not correspond with the origin of the plume, we decided to take as our plume origin whichever is upwind of either the "upwind" end of the XCH4 mask (cyan dot) or the center of mass of the positive pixels of the flux mask (green dot). The top left panel of Figure S1.2 shows that the algorithm chooses the upwind end of the XCH4 mask (blue dot) as the plume origin, while in the bottom left panel, it chooses the flux clump center (green dot) as the origin of the plume.

Each plume was quantified using a 2nd application of the DI method, this time for boxes surrounding the plume origin and expanding in size, which we call the growing box method (detailed in Chulakadabba et al., 2023). A series of rectangles were drawn surrounding the source, with one side of the box crossing the plume at a range of distances (Figure S1.3). For each rectangle, the flux was calculated according to Equation S1.1. By averaging the flux for the plume at many distances, we arrive at a robust flux estimate for the source. The flux calculation used the wind speed from HRRR; if the plume was sufficiently elongated and with highly elevated XCH4, the wind direction was determined by the long axis of the plume. Specifically, the wind direction was obtained from the plume angle if the eccentricity of the plume was greater than 0.87 and the XCH4 mask contained >200 connected 10 m × 10 m pixels that are above 1.7*[standard deviation of cropped scene's XCH4] + [mean of cropped scene's XCH4]. If these conditions were not met, the HRRR wind direction was used. We used the wind direction information in the plume image because errors in wind direction can have a significant impact on calculated flux. The rectangles used in the flux calculation were rotated along the direction of the wind.

The size of the rectangle was increased sequentially by one pixel (10 m) in each direction, with the exception of the upwind side, which was increased by a pixel for every fourth rectangle to avoid catching other sources yet still average over the background. The flux for each rectangle as a function of distance from the source to the upwind edge of the rectangle is shown in Figure S1.3 right. Boundary layer eddies break up the plume structure, leading to a buildup of methane concentration in some areas and depletion in others. Since these eddies are not resolved by HRRR, we see oscillations of the computed flux values as a function of distance, on the scale of the associated structures. By averaging the flux over the range of distances, we arrive at a robust flux estimate for the source that averages over the eddy-scale variability of the winds. The estimated flux for the individual source is the average flux for all rectangles crossing the plume, which may not be all rectangles for which the flux is initially calculated. We average the flux starting with the first rectangle whose flux is greater than 0.5*(the median of all rectangles' fluxes), and ending with the last rectangle whose flux is greater than 0.5*(the median of all rectangles' fluxes) - the rectangles used in this average have a black dot in Figure S1.3 right. The uncertainty in the flux estimate is calculated from the standard deviation of all points with a dot.

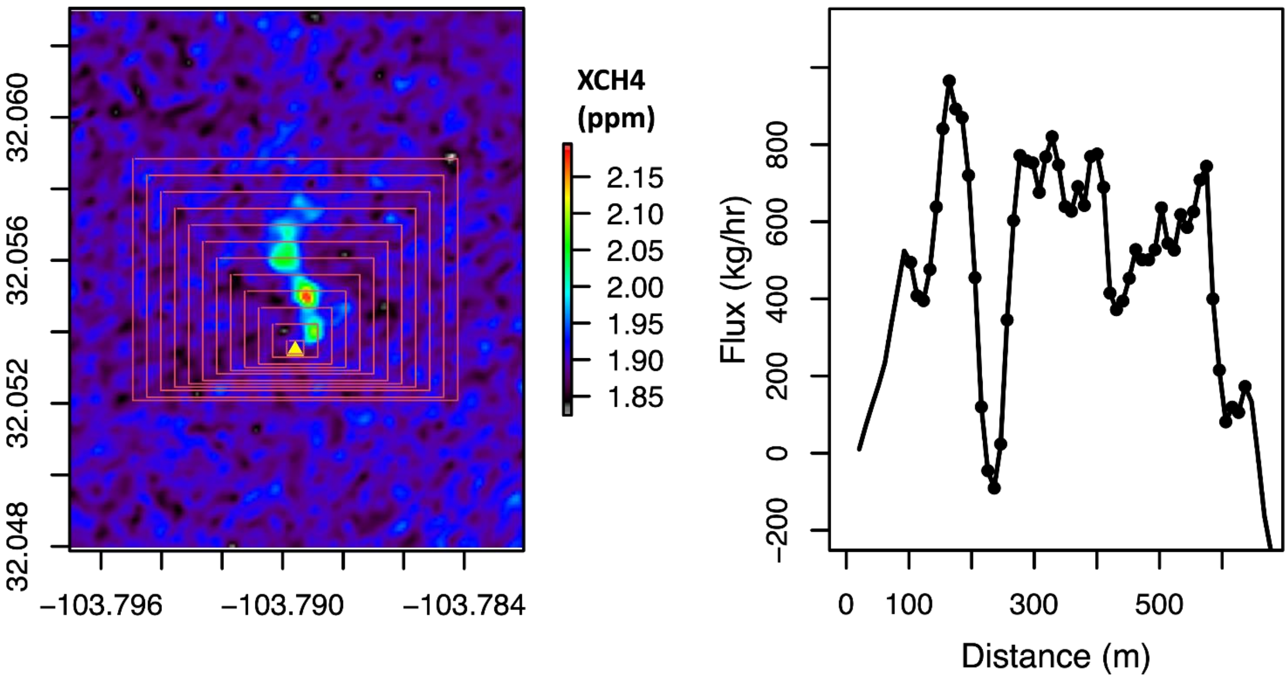

Figure S1.3 Left: MethaneAIR image of an oil and gas plume in the Permian basin observed on 6 August 2021. The likely source location of the plume found by the plume-finder algorithm is shown as a yellow triangle; every 5th rectangle of those used to calculate the flux divergence is shown in red. Right: Calculated flux divergence as a function of distance from the source to the downwind edge of the rectangle. The fluctuations of the apparent flux with distance from the source reflect the influence of eddy-scale motion as well as contributions of excess methane from nearby sources. The influence of eddy-scale motions is evident in the oscillation at approximately 250m intervals, the apparent length scale for eddies at this overpass. The surface flux is estimated by averaging the flux divergence over several eddy scales to average out dm/dt. Dots indicate data points which are averaged to calculate the mean flux for this plume of 452 kg h^{-1}. The uncertainty in the flux estimate is calculated as the standard deviation of the points with dots.

Sensitivity studies were conducted to find the combination of parameters that led to the greatest number of verifiable plumes found, with a reasonable fraction (<60%) of false positives. Plumes were considered valid if the plume was associated with identifiable infrastructure and appeared visually comparable to prior plumes detected by the platform, including those verified by controlled release testing. The size of the box used to calculate the gridded flux divergence product was tested over values ranging from 200 to 800 m. The thresholds for masking gridded DI "clumps" and XCH4 plumes were tested for values from 1 to 2.4 times the standard deviation of the scene's gridded flux or XCH4. The number of contiguous DI pixels required for a plume detection was varied from 8 - 36; the number of contiguous XCH4 pixels required for a plume detection was varied from 100 to 500. The values tested, results, and parameters chosen are shown in Table S1.1. We thoroughly tested scenes in the Permian, Appalachian, and Haynesville basins because these areas have differing surface albedos and wind speeds, and numerous visible plumes. These values will need to be reassessed for different platforms - for example MethaneSAT, which had more coarse resolution than MethaneAIR, required a separate sensitivity study and different values for these parameters.

Table S1.1 Sensitivity test results used to determine adjustable parameters for the plume finder algorithm. ’Gridded DI box size’ is the length of the box around which DI is calculated in m (boxes are oversampled, so gridded DI product is on a grid of x/3 m). ‘Sigma DI’ and ‘Sigma XCH4’ are the multipliers for the standard deviation of scene’s gridded flux or XCH4, respectively, which are used as a threshold to find elevated DI or XCH4 masks. ‘nmin DI’ and ‘nmin XCH4’ are the minimum number of contiguous gridded DI pixels and XCH4 pixels, respectively, above the threshold required to keep a DI or XCH4 mask. The number of ‘Good’ plumes found are those that pass our manual QAQC, while the ‘Total’ is the total number of plumes found by the algorithm, and ‘Fraction’ is good/total plumes. We chose to use the parameters in bold because they maximized the number of ‘good’ plumes found while having a fraction of good/total plumes greater than 40%.

Adjustable Parameters					**Permian (RF06)**			**Appalachian (MX043)**			**Haynesville (MX017)**			**Combined Flights**		
Gridded DI box size (m)	sigma DI	sigma XCH4	nmin DI	nmin XCH4	Good	Total	Fraction	Good	Total	Fraction	Good	Total	Fraction	Good	Total	Fraction
200	1.3	1.3	8	125	41	729	0.06							41	729	0.06
200	1.3	1.3	24	200	37	208	0.18	25	126	0.20	16	90	0.18	78	424	0.18
200	1.6	1.6	20	200	32	110	0.29	23	61	0.38	13	31	0.42	68	202	0.34
200	1.6	1.6	36	200	26	63	0.41	16	29	0.55				42	92	0.45
400	1.3	1.3	24	200	30	84	0.36	23	60	0.38	12	31	0.38	65	175	0.37
400	1.4	1.4	24	175	30	72	0.42	22	60	0.37	13	32	0.41	65	164	0.40
400	1.6	1.6	20	200	29	48	0.61	21	32	0.64	13	21	0.63	63	101	0.62
600	1	1	12	200	37	152	0.24	29	174	0.17	13	114	0.11	79	440	0.18
600	1	1	20	300	27	42	0.65	19	31	0.61	11	20	0.55	57	93	0.62
600	1	1.4	16	200	31	58	0.52	19	39	0.50	10	27	0.36	60	125	0.48
600	1.3	1.3	8	125	37	135	0.27	30	165	0.18	13	97	0.13	80	397	0.20
600	**1.3**	**1.3**	**12**	**200**	**32**	**70**	**0.46**	**22**	**61**	**0.36**	**12**	**30**	**0.40**	**66**	**161**	**0.41**
600	1.3	1.3	16	250	26	57	0.45							26	57	0.45
600	1.3	1.3	24	500	21	33	0.65							21	33	0.65
600	1.4	1.4	8	200	29	73	0.40	23	57	0.40	13	32	0.41	65	162	0.40
600	1.6	1.6	12	200	27	45	0.61	19	34	0.57	9	25	0.36	56	104	0.54
600	1.8	1.8	16	250	18	28	0.64							18	28	0.64
600	2.4	2.4	8	100	24	28	0.86	15	21	0.71	8	19	0.42	47	68	0.69
800	1.3	1.3	8	200	27	65	0.42	20	62	0.33	11	29	0.38	58	156	0.37

S2. Facility-level attribution and repeat detection identification methods

Attribution of point sources to facility types has been achieved through spatially querying known infrastructure locations (Hmiel et al. 2022), or by manually review of available imagery (Cusworth et al 2022). Here we apply both methods. First, we assembled a collection of public infrastructure databases, including state and federal level inventories of air emission sources(Active Air Pollution Emitting Facilities; New Mexico Environment Department Data; Ohio Emissions Inventory point source data; Coal Mining Operation - Underground Mines; West Virginia Department of Environmental Protection GIS Data; Underground and Surface Coal Mines), and O&G infrastructure collections (Omara et al. 2023) and several sources dedicated to other methane emitting sectors (LMOP Landfill and Project Database; Coal Mining Operation - Underground Mines; CAFOs in the US; Mineral Resources of Wyoming).

Infrastructure databases typically represent facilities as point locations, so joining the origin of a plume must account for variability in where the single point representing the facility is located within the facilities footprint. For facilities with a small footprint, like O&G well sites, spatially joining the plume origin to the single known-infrastructure point is more straightforward compared to a large footprint facility, such as a processing plant. Conversely, the density of different facilities, such as a wellsite in close proximity to a compressor station, can pose a problem when using excessively large spatial buffers to query known locations and make a singular determination. To address both issues, we used a series of consecutive spatial buffers in combination with a prioritization hierarchy based on typical footprint sizes of the facilities to make a single attribution of facility type.

Features within this assembled infrastructure database were searched within successive distances of 150m, 300m, and 500m radii around all point source identifications. If no facility was found within a 150m radius, then the database was queried again at 300m and so on. If two or more features were identified within a given radius, a priority was given to the feature according to this facility type hierarchy corresponding to facility footprint size:

processing, CAFO > compressor station, waste, coal > tank battery, other > O&G wells

If multiple features were identified within the same level of the hierarchy, then the closest of these infrastructure points was used for the attribution. These attributions were then manually reviewed alongside available satellite or streetview imagery. For cases where a facility type could not be determined, such as where the plume was ambiguously between two facilities of different types, or no information nor recent imagery was available on the underlying location, the attribution was left as unknown. If the plume was between two facilities of the same sector during manual review, such as between an O&G well and a compressor station, then the sector was noted but specific attribution left as unknown. All point source detections were then spatially aggregated within a 300 m radius to identify both the number of unique locations where emissions were detected, and locations where emissions were detected multiple times across individual flights. Attributions across the aggregated detections were then manually reviewed for consistency to one another as an additional QAQC step for attribution and aggregation to a single facility.

Definitions for attributed facility types are as follows:

Compressor stations: facilities that use compressors to send produced gas along a pipeline network. While some production sites do have compressors on-site, these facilities do not have wellheads. A distinction between gathering and boosting segment stations, and transmission and storage segment stations is not made.

O&G wellsites: includes pumpjack-only sites and wellpads with other complex equipment present. While assembling infrastructure databases, it was noted that the delineation of a pad with a centralized tank battery, used for gathering production from multiple wellsites, was not consistent. In some regions or sources, centralized tank batteries were defined specifically while elsewhere they were referred to as just wellsites. Due to this inconsistency, we include centralized tank batteries in this category, despite the possibility that emissions characteristics may differ.

Pipelines: natural gas pipelines at least 150m from any pad. A distinction is not made between gathering and transmission pipelines.

Processing: facilities that ready natural gas for distribution by further separating liquids, heavier hydrocarbons, and other contaminants.

Waste: municipal and industrial waste landfills and their associated treatment facilities

Coal: Any facility related to coal mining, such as a mine entryway or vent.

CAFO: Concentrated animal feeding operations, such as for dairy or beef production.

Other: Any other non-O&G sector facilities, such as power plants.

S3. Sub-basin regions of interest

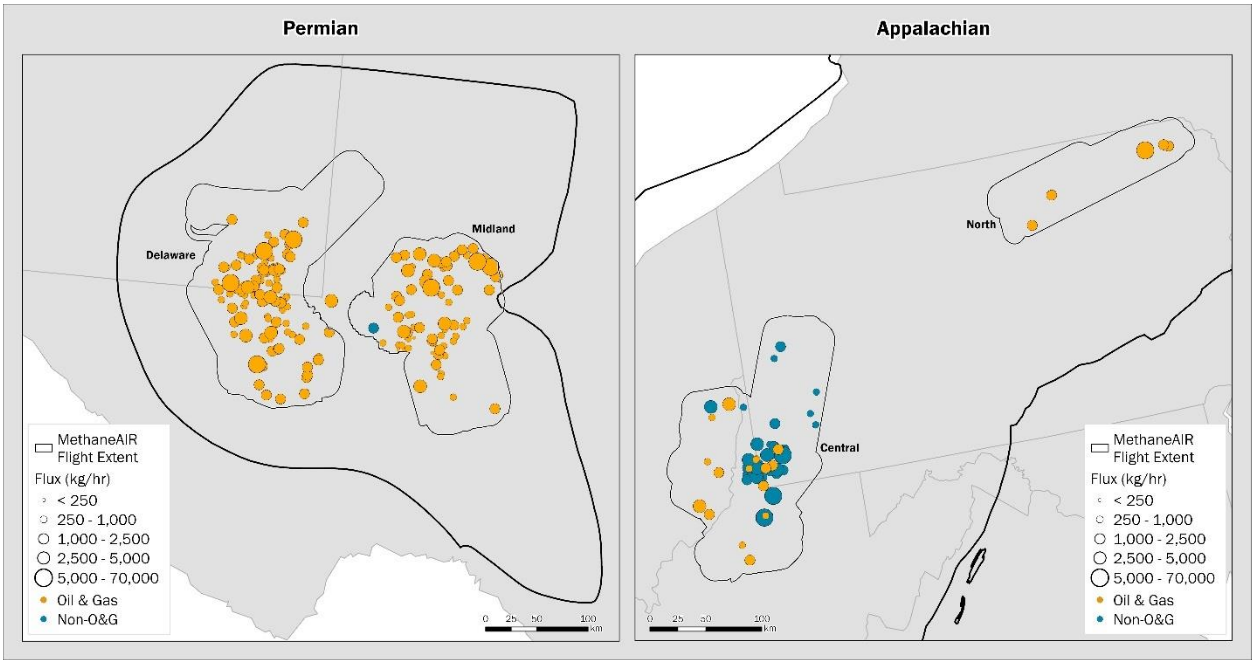

Figure S3.1 Discussed sub-regions within the Permian and Appalachian. Bold outlines indicate basins while gray outlines indicate regions flown by MethaneAIR without the inbound and outbound flight tails.

S4 . Calculation methods for point source emissions totals and MC Simulation

Studies using point source data to derive basin level estimates of emissions have commonly used some form of persistence, the number of times a source was detected vs observed to weight or average observed emissions (Cusworth et al. 2022; Chen Sherwin et al. 2022). The logic behind this weighting is that point source emissions magnitude can be highly variable both across its emitting duration and occurrence. Due to this variability, a sources contribution to an estimate of basin wide emissions should be weighted across all positive or negative detections or overflights. In the event where there are limited overflights of a given source, an additional step has been taken to use a monte-carlo simulation to randomly sample a distribution of persistence values according to observations from the same facility type and basin.

Our calculation approach for basin level point source emissions in this study is equivalent to a by-day persistence weighting approach, albeit without the additional step of monte-carlo simulations for sources with limited overflights. Our justification is that this study explores several basins either new or underrepresented the methane point source literature, and thus we do not have a preexisting extensive sample of representative persistence values to sample. Additionally, operator practices and emissions can change quickly over time, so it would be an additional assumption to apply persistence values from prior studies in overlapping regions.

The most heavily studied O&G basin in the literature is the Permian basin in Texas and New Mexico (Cusworth et al. 2021; Cusworth et al. 2022; Chen Sherwin et al. 2022; Kunkel et al. 2022). To test the possible effects of MC simulation in MethaneAIR basin level point source estimates, we compared approaches with and without MC simulation for sources with three or less flyovers. We used all available Permian persistence values collected by the AVIRIS NG and GAO platforms from 2019-2021 (Cusworth et al. 2022) and simulated persistence using the average across 10,000 random draws for the same facility type and subbasin. We compared the simulations effect on both basin-level total point source emissions magnitude and the relative contribution of facility types for observations from MethaneAIR in 2023 (Table S2.1)

Table S4.1 Comparison of monte-carlo simulation treatments for persistence weighting. Values in parenthesis indicate simulated 95% confidence interval. * indicates significant differences between treatments defined by no overlap in the 95% confidence interval.

	Average point source emissions for all sources (t/h)	Percent contribution 95% confidence interval by facility type				
		Compressor station	Wells	Pipeline	Processing plant	Unknown
Delaware						
MC simulation	47 (31 – 64)	19 – 32	16 – 26	4.3 – 71	3.7 – 16	2.1 – 6.9
No MC simulation	60 (42 – 78)	21 – 37	17 – 32	4.1 – 56	3.6 – 14	3.3 – 9.2
Midland						
MC simulation	*23 (18 – 29)	17 – 48	30 – 57	3.2 – 19	4.2 – 18	0 – 1.9
No MC simulation	*54 (42 – 65)	17 – 39	35 – 65	3.4 – 19	3.2 – 13	0 – 2.74

With MC simulation the overall magnitude of Midland emissions is significantly smaller such that there is no overlap with the confidence interval with the no-MC treatment. This is due to the fact that the four 2023 Midland flights yielded mostly areas with two repeat overflights of each source, and thus the entire Midland sample underwent MC simulation. In the Delaware, the MC treatment has again a lower emissions magnitude, but there is overlap in the confidence interval between treatments.

This is likely because the core area of the Delaware and much of the southern portion was overflown three or more times, and thus the majority of the sample did not undergo MC simulation in both treatments. Despite the shifts in the magnitude, the relative proportion of emissions by facility type remains similar across both treatments, with overlaps in the confidence intervals across all types. From this exercise, we conclude that the overall magnitudes of emissions should not be compared using the differing methodologies, however, we expect results comparing the relative sectoral contributions of emissions to remain similar regardless of methodology.

S5. Observational frequency and threshold for comparison

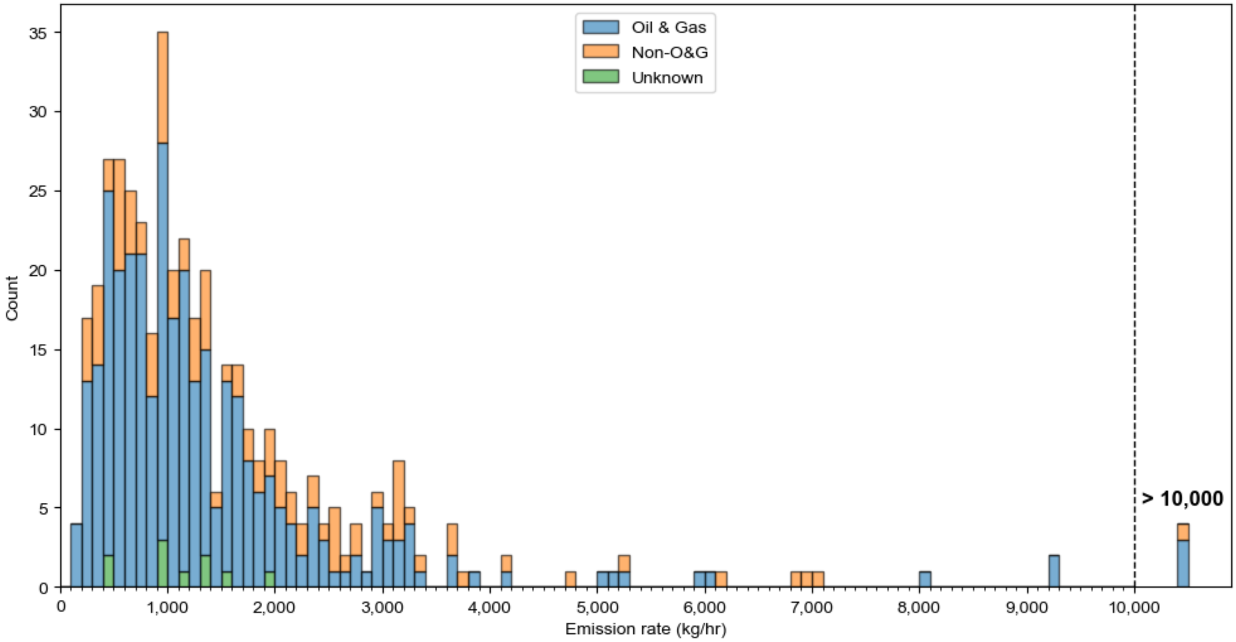

Figure S5.1 Observed emission rate distribution of all MethaneAIR detections by industry sector. Right hand side represents all plumes above 10,000 kg/h.

As mentioned previously, to meaningfully explore the relative contributions of sources, we must attempt to minimize the effect of present but unidentified sources across all scenes. Setting a threshold allows us to create a more definitive comparison that can be aligned with observations from other sensors if their sensitivity meets the same threshold. In single-blind controlled release testing, MethaneAIR has identified point sources as small as 33 kg h^{-1}, but this detection likely did not represent a high probability of detection generally. Instruments do not have fixed probabilities of detections for point sources. Rather, the probability of detecting a point source is dependent on the emission source rate, in-situ conditions, and applied processing methods, and thus variable with each emission source in a given scene. Determining the probability of detection for all point sources given the observed conditions in MethaneAIR campaigns, and if differing processing protocols using other instruments would perform at the same threshold is outside the scope of this work. However, we can take a simpler approach using some assumptions on the differences between observed and assumed emissions distributions. Anthropogenic methane emission sources follow a lognormal distribution (Zavala-Araiza et al., 2015), and thus the number of expected sources should increase as emission rate decreases. Therefore, the peak in observed emissions distribution should indicate a threshold at which unidentified sources begin to have an effect on observed distribution (Figure S5.1).

To estimate this emission rate threshold at which we observe a drop in the ability of MethaneAIR to confidently detect a point source emission, we used fit the empirical point source data from MethaneAIR to a lognormal distribution and extracted the distribution parameters. Next, we use the extracted parameters of the lognormal distribution to simulate 10,000 new point source emission rates, which were then sorted into 50 kg h^{-1} bins from 50 to 5,000 kg h^{-1}, which was repeated 1,000 times. We replicated this process again while excluding point sources emitting above 10,000 kg h^{-1} to examine the impact of excluding these abnormally high emitting point sources relative to the majority of point source detections. We then assumed the emission rate bin at which the count of simulated point source emissions begins to drop as our estimated emission rate threshold.

Simulated emissions peaked at 550-600 kg h^{-1} using all MethaneAIR point source observations, and at 600-650 kg h^{-1} when sources greater than 10,000 kg/hr were excluded. Using the results of these two approaches, we set the threshold for comparison as a conservative value of 550 kg h^{-1} since we observed no clear reason to account for the abnormally high emissions separate from the full suite of point source emissions. The probability of detecting a point source is dependent on several factors, such as the emission source rate, in-situ environmental conditions, topographical factors (e.g., land cover), and applied processing methods. Therefore, this approach for estimating threshold for comparison is likely a broad representation of the true emission rate threshold. Future work should investigate how the instrument's probability of detecting a point source changes across these variables.

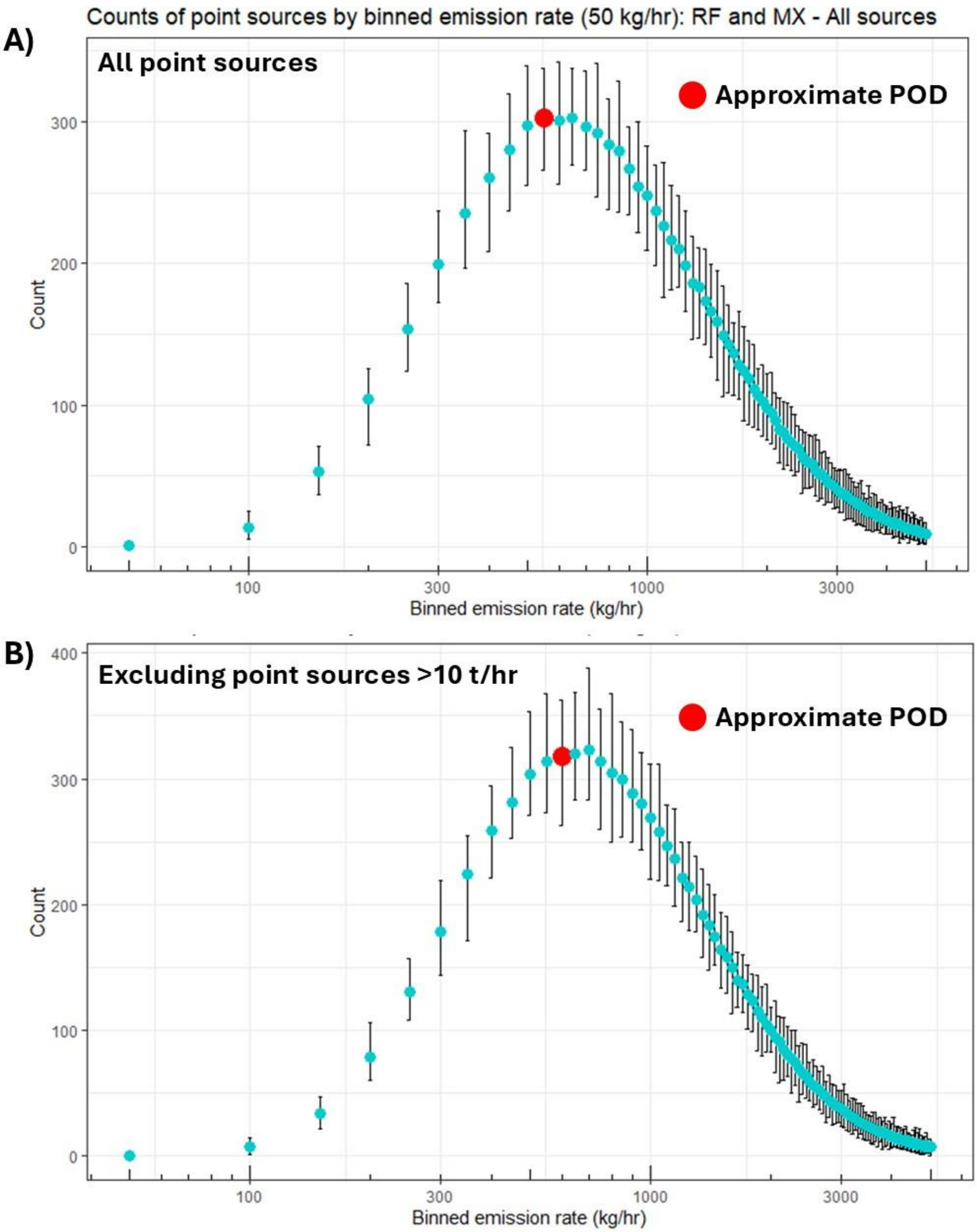

Figure S5.2 Simulated distributions of point source emissions binned at 50 kg h^{-1} intervals using A) all detected point sources and B) excluding point sources with emission rates >10 t h^{-1}.

Emissions between the minimum detection and quantification of the methodology used in this study (150 kg h^{-1}) and the threshold for comparison (550 kg h^{-1}) represent a partial detection range, at which plumes of this size class are present but possibly not entirely accounted for to a high degree of certainty. To estimate the effect of the contribution of this partial detection range, we segment the 2023 basin level total point source emission results (Figure 4) by above and below the threshold for comparison (Figure S5.3). Overall, we find that the partial detection range has a minimal effect on estimated point source emissions, contributing only ~2.4% of the total flux estimate for 2023.

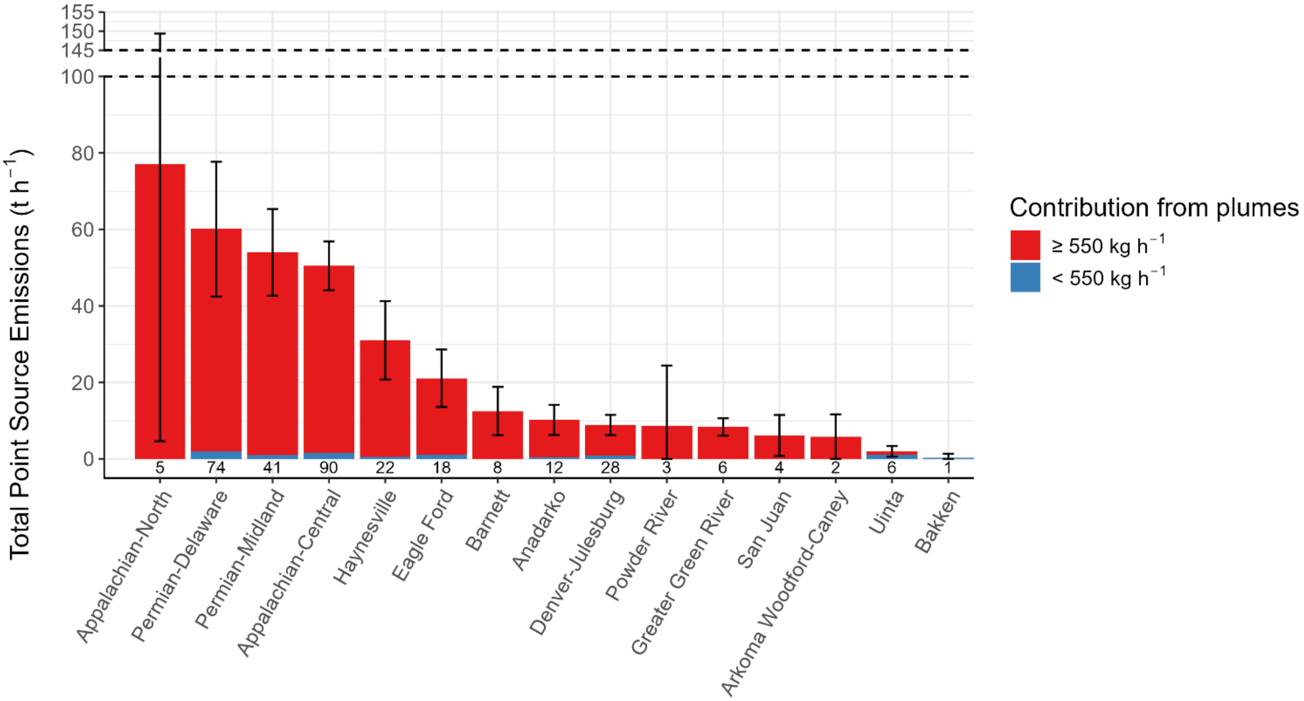

Figure S5.3 Average basin-level emissions totals for all high-emitting methane point sources detected by MethaneAIR in 2023. Colors indicate flux contribution from sources within the partial detection range (blue) and above the threshold for comparison (red). Numbers below the stacked bar chart represent total plume sample size. Error bars represent the 95% confidence interval of the basin-level total emissions for all high-emitting methane point sources. Note the axis break between 100 t h^{-1} and 145 t h^{-1}.

S6. Daily variation of basin sub-basin regions

To retrospectively explore the needed number of overpasses that would contribute to a robust estimate of high-emitting point source emissions, we compare daily emission estimates in sub-basin regions of the Appalachian-Central and Denver-Julesburg that were flown on five and six separate days during the 2023 campaign.

For the Appalachian-Central subregion (Figure S6.1), daily and aggregate emission estimates all overlap with one another given their respective 95% confidence intervals. This result is in part due to the large uncertainty ranges on the day-to-day estimates. However, any combination of two days would produce a total flux estimate without uncertainty that is within the confidence interval of the five-day estimate. We interpret these results to mean that for the emissions observed by MethaneAIR using these processing methods, one to two sampled days would produce a representative estimate of point source emissions for this subregion. Whether or not this interpretation applies to the entire basin would depend on changes in the observed facility composition and source intermittency going from the subregion to basin scale.

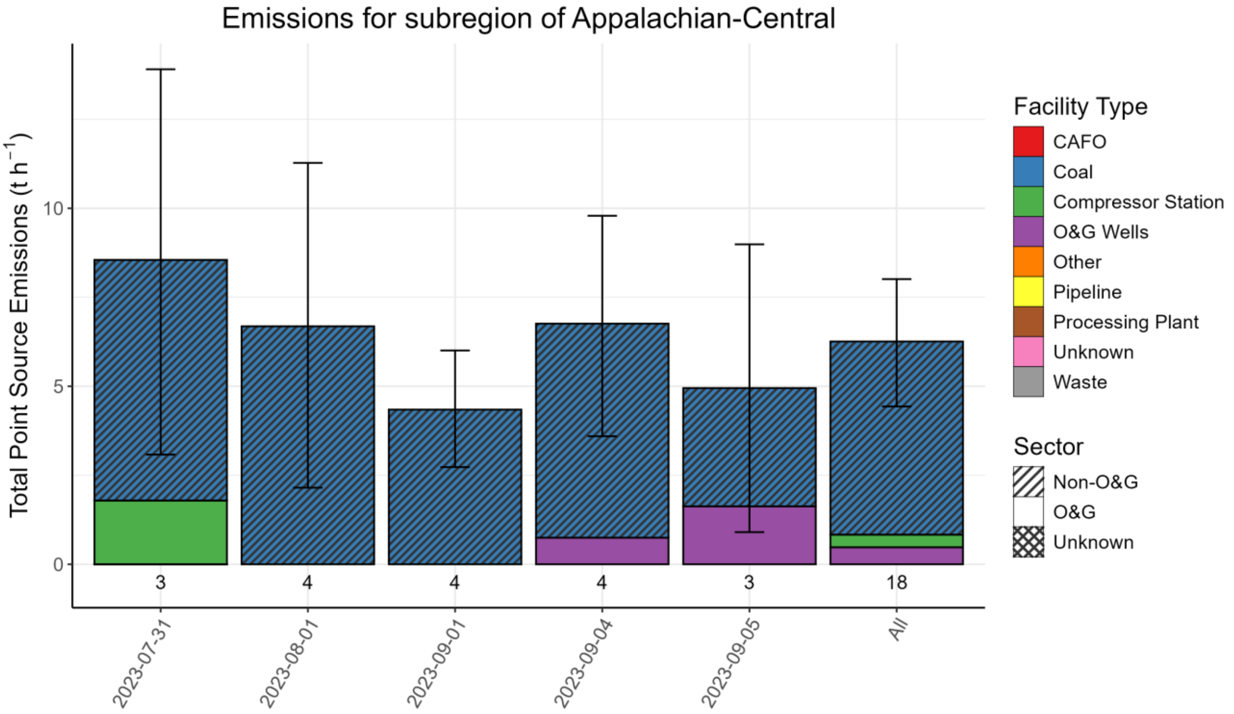

Figure S6.1 Daily variation of point source emission from a subregion of the Appalachian-Central. All represents the total point source emission estimate using all days with persistence weighting.

Conversely, results in the subregion of the Denver-Julesburg show a much larger degree of day-to-day variation (Figure S6.2). Observations from 10-09-2023 and 10-13-2023 are comparatively lower than the estimate from 06-22-2023, which had a single processing plant plume (~8 t h^{-1}) contributing most emissions on that day. Additionally, we cannot rule out the possibility of changes due to seasonal variation in the approximately three-month time period between the first and last flights. The range in the flux estimation without uncertainty using any combination of five out of six sampling days produces a larger range than that of the 95% confidence interval of the estimate using all six days. Assuming the observed variation is strictly due to the intermittency of methane point sources and not seasonality, we interpret this result to signal that several sampling days, possibly five or more depending on the desired level of uncertainty, are required to estimate total point source emissions in this emission rate range for this subregion.

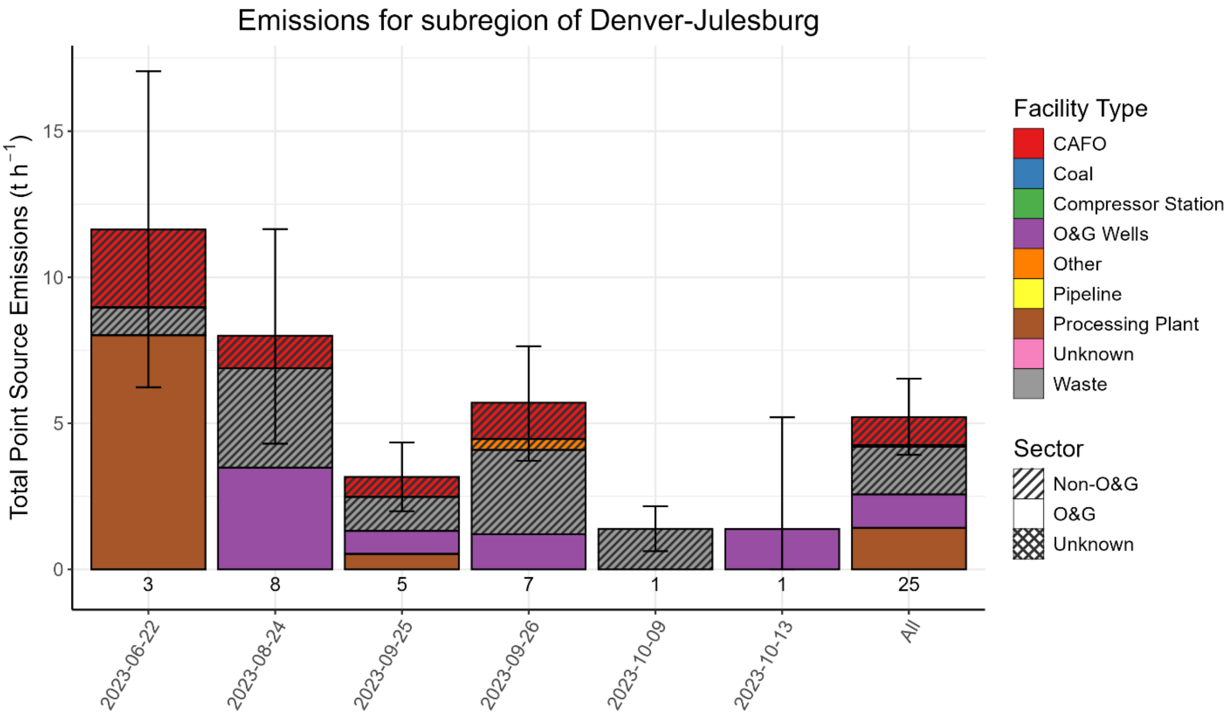

Figure S6.2 Daily variation of point source emission from a subregion of the Denver-Julesburg. All represents the total point source emission estimate using all days with persistence weighting.

Our results in the Appalachian and Denver-Julesburg basins, although from different basins with very different facility type composition, suggest that required temporal sampling will vary by basin and possibly by subregion. This finding is consistent with results from Chen et al. 2024, which indicated that emissions characteristics in the production core vs periphery of the New Mexico Permian were significantly different, and that one comprehensive overflight may not be enough to estimate emissions depending on the desired accuracy. While only one daily estimate, 10-09-2023, produced an uncertainty range that did not overlap with the uncertainty range using all observed days, this result is primarily driven by large uncertainty ranges of daily and aggregate emissions estimates and not necessarily justification for the application of an ergodic hypothesis based on one comprehensive overflight.